Neurobiology of Disease

Abnormal Cortical Complexity and Thickness Profiles Mapped in Williams Syndrome

Paul M. Thompson,[1] Agatha D. Lee,[1] Rebecca A. Dutton,[1] Jennifer A. Geaga,[1] Kiralee M. Hayashi,[1] Mark A. Eckert,[2] Ursula Bellugi,[3] Albert M. Galaburda,[4] Julie R. Korenberg,[5] Debra L. Mills,[6] Arthur W. Toga,[1] and Allan L. Reiss[2]

[1]Laboratory of Neuroimaging, Brain Mapping Division, Department of Neurology, University of California Los Angeles School of Medicine, Los Angeles, California 90095, [2]Stanford Psychiatry Neuroimaging Laboratory, Department of Psychiatry and Behavioral Sciences, Stanford University School of Medicine, Stanford, California 94305, [3]Salk Institute Laboratory for Cognitive Neuroscience, La Jolla, California 92037, [4]Department of Neurology, Harvard Medical School, Boston, Massachusetts 02215, [5]Department of Pediatrics, University of California Los Angeles, Los Angeles, California 90095, and [6]Department of Psychology, Emory University, Atlanta, Georgia 30322

We identified and mapped an anatomically localized failure of cortical maturation in Williams syndrome (WS), a genetic condition associated with deletion of ~20 contiguous genes on chromosome 7. Detailed three-dimensional (3D) maps of cortical thickness, based on magnetic resonance imaging (MRI) scans of 164 brain hemispheres, identified a delimited zone of right hemisphere perisylvian cortex that was thicker in WS than in matched controls, despite pervasive gray and white matter deficits and reduced total cerebral volumes. 3D cortical surface models were extracted from 82 T1-weighted brain MRI scans (256 × 192 × 124 volumes) of 42 subjects with genetically confirmed WS (mean ± SD, 29.2 ± 9.0 years of age; 19 males, 23 females) and 40 age-matched healthy controls (27.5 ± 7.4 years of age; 16 males, 24 females). A cortical pattern-matching technique used 72 sulcal landmarks traced on each brain as anchors to align cortical thickness maps across subjects, build group average maps, and identify regions with altered cortical thickness in WS. Cortical models were remeshed in frequency space to compute their fractal dimension (surface complexity) for each hemisphere and lobe. Surface complexity was significantly increased in WS ($p < 0.0015$ and $p < 0.0014$ for left and right hemispheres, respectively) and correlated with temporoparietal gyrification differences, classified via Steinmetz criteria. In WS, cortical thickness was increased by 5–10% in a circumscribed right hemisphere perisylvian and inferior temporal zone ($p < 0.002$). Spatially extended cortical regions were identified with increased complexity and thickness; cortical thickness and complexity were also positively correlated in controls ($p < 0.03$). These findings visualize cortical zones with altered anatomy in WS, which merit additional study with techniques to assess function and connectivity.

Key words: **Williams syndrome; brain imaging; genetics; MRI; cortex; fractal complexity; brain mapping**

Introduction

Williams syndrome (WS) is an enigmatic disorder associated with a genetic deletion in the 7q11.23 chromosomal region (Korenberg et al., 2000), with an estimated incidence of 1 in 20,000 live births (Duba et al., 2002). WS subjects have disrupted cortical development and mild to moderate mental retardation but have relative proficiencies in language skills, social drive, and musical ability (Bellugi et al., 2000). The genetic deletion typically causes cardiovascular and facial anomalies, neonatal hypercalcemia, and impaired cognitive development in infancy (Trauner et al., 1989).

Received Sept. 8, 2004; revised March 14, 2005; accepted March 15, 2005.

This work was supported by grants from the National Institute for Biomedical Imaging and Bioengineering, by National Center for Research Resources Grants R21 EB01651 and R21 RR019771 (P.M.T.), by National Institute of Mental Health (NIMH) Grant K02 MH01142 (A.L.R.), and by National Institute of Child Health and Human Development Grants R01 HD31715 (A.L.R.) and P01 HD33113 (A.L.R., J.R.K., D.L.M., A.M.G., U.B.). Additional support was provided by Human Brain Project Grants P20 MH/DA52176 and P41 RR13642 (A.W.T.) to the International Consortium for Brain Mapping funded by NIMH and the National Institute on Drug Abuse.

Correspondence should be addressed to Dr. Paul Thompson, Laboratory of Neuroimaging, Department of Neurology, University of California Los Angeles School of Medicine, Room 4238, Reed Neurological Research Center, 710 Westwood Plaza, Los Angeles, CA 90095-1769. E-mail: thompson@loni.ucla.edu.

DOI:10.1523/JNEUROSCI.0165-05.2005

 0270-6474/05/254146-13$15.00/0

Progress in understanding how this genetic deletion impacts brain structure and behavior is impaired by the lack of detailed maps establishing the scope and anatomical extent of brain anomalies in WS. Quantitative maps of cortical integrity may also narrow down when and where altered gene expression impacts cortical development *in utero*, and which circuitry underlies the cognitive and behavioral imbalance in WS. Gyrification is thought to be disturbed in WS, but current measures, from two-dimensional (2D) serial sections (Zilles et al., 1988; Schmitt et al., 2002), depend on brain orientation and the direction of image slicing. Postmortem studies in small samples have shown multiple small gyri on the dorsal cortical surface, but the regional specificity of these changes has not been mapped (Galaburda and Bellugi, 2000; Galaburda et al., 2001).

MRI findings

WS subjects have reduced overall gray matter (GM) and white matter (WM) volumes, with disproportionate decreases in the thalamus and occipital lobes (Reiss et al., 2004). It is unclear whether the WS genetic deletion impacts the cortex diffusely or focally, because volumetric increases have also been found in the

amygdala, and superior temporal and orbitofrontal gyri in WS (Reiss et al., 2000, 2004). WS subjects show relative strengths in functions typically localized to perisylvian cortices (verbal and musical ability) and the fusiform face area (face processing), although they do not perform on a par with normal age-matched controls, and they are more severely impaired in parietal-occipital lobe functions such as visuospatial processing. We therefore hypothesized that areas in the dorsal processing stream might show greater cortical thinning than the adjacent perisylvian cortex.

Overview of study and goals

We therefore set out to create the first detailed cortical thickness maps in WS, using a magnetic resonance imaging (MRI) brain image database ($n = 82$). We developed a new method that creates group average maps of cortical thickness over the entire human cortex. Color-coded maps show the magnitude and spatial extent of cortical disruption. To empower the analysis, we used cortical pattern matching (Thompson et al., 2003) to disentangle variations in sulcal patterning and thickness. This approach adjusts for large individual variations in cortical organization that obscure group or genetic differences in cortical structure (Thompson et al., 2001b).

We also improved the analysis of gyrification to measure cortical complexity for the first time in three dimensions and compared it regionally across groups. We extended the notion of fractal complexity to three-dimensional (3D) cortical surfaces, adapting to complex individual variations in cortical folding and sulcal patterning. We hypothesized that temporal/parietal and occipital complexity would be altered in WS. Finally, we related these differences to classical gyrification measures using Steinmetz criteria (Steinmetz, 1996) to evaluate their anatomical correlates.

Materials and Methods

Participants. Subjects and brain-scanning protocols were used exactly as in the study by Reiss et al. (2004). Exclusion criteria included a history of medical conditions not typically associated with WS, such as epilepsy or other neurological conditions. All WS participants were evaluated at the Salk Institute (La Jolla, CA) as part of a program project on genetics, neuroanatomy, neurophysiology, and cognition. WS diagnosis was genetically confirmed in all cases by fluorescent *in situ* hybridization, which tested for deletion of one copy of the elastin gene on chromosome 7. A total of 42 subjects with genetically confirmed Williams syndrome (mean $\pm$ SD, 29.2 $\pm$ 9.0 years of age; range, 12–50 years of age; 19 males, 23 females) and 40 age-matched healthy controls (27.5 $\pm$ 7.4 years of age; range, 18–49 years of age; 16 males, 24 females) were included in the study. Wechsler Full-Scale intelligence quotient (IQ) scores were available for 41 of the 42 WS subjects (mean, 68 $\pm$ 9; range, 46–83); the two untested subjects exhibited similar levels of cognitive function on other measures. As in the study by Reiss et al. (2004), healthy control subjects (with no history of major psychiatric, neurological, or cognitive impairment) were recruited at both the Salk Institute and Stanford University. Control subjects were further screened to rule out any history of learning, language, or behavioral disorder. The majority of controls in the study did not have IQ testing performed. Those that did ($n = 16$) had a mean full-scale IQ of 104 with an SD of 12 (range, 86–126). All procedures were approved by the Institutional Review Boards of both institutions, and all participants provided informed consent (and parents or guardians provided written consent where appropriate).

MRI scanning. 3D MRI brain images were collected using a GE-Signa 1.5 T scanner (General Electric, Milwaukee, MI). The same 3D spoiled gradient echo pulse sequence was used for all participants, with the following parameters: echo time, 5 ms; repetition time, 24 ms; flip angle, 45°; number of excitations, 2; matrix size, 256 $\times$ 192; field of view, 24 cm; slice thickness, 1.2 mm; 124 contiguous slices. Scans were analyzed at the University of California Los Angeles Laboratory of Neuroimaging by image analysts blinded to all subject information, including age, gender, and diagnosis. All MR images were processed with a series of manual and automated procedures that are described in detail in other studies and summarized below. [Cortical surface analyses were identical to those described by Thompson et al. (2003, 2004), except for the thickness and complexity analyses, which are detailed below.]

Image processing. First, nonbrain tissue (i.e., scalp, orbits) was removed from the images, and each image volume was resliced into a standard orientation by a trained operator (A.D.L.) who "tagged" 20 standardized anatomical landmarks in each subject's image data set that corresponded to the same 20 anatomical landmarks defined on the International Consortium for Brain Mapping-53 average brain (Mazziotta et al., 2001; Thompson et al., 2003). Next, brain image volumes were more carefully spatially registered to each other by defining 144 standardized, manually defined, anatomical landmarks (72 in each hemisphere; the first and last points on each of 36 sulcal lines drawn in each hemisphere are described below) in every individual (Sowell et al., 2003a). A least-squares, rigid-body transformation spatially matched each individual to the average of all of the healthy controls. In this way, every individual's brain was matched in space, but global differences in brain size and shape remained intact. Automated tissue segmentation was conducted for each volume data set to classify voxels as most representative of gray matter, white matter, CSF, or a background class (representing extracerebral voxels in the image) on the basis of signal intensity. The procedure fits a mixture of Gaussian distributions to the intensities in each image before assigning each voxel to the class with the highest probability (Shattuck et al., 2001). Then each individual's cortical surface was extracted and three-dimensionally rendered using automated software (MacDonald, 1998). This software creates a mesh-like surface that is continuously deformed to fit a threshold intensity value for the cortical surface that was defined as the MRI signal value, which best differentiated cortical CSF from the underlying cortical gray matter. Each resulting cortical surface was represented as a high-resolution mesh of 131,072 surface triangles spanning 65,536 surface points.

Anatomical analysis. An image analysis technique, known as cortical pattern matching (Thompson et al., 2003), was used to localize disease effects on cortical anatomy and increase the power to detect group differences. The approach models, and controls for, gyral pattern variations across subjects. A set of 72 sulcal landmarks per brain constrains the mapping of one cortex onto another. This associates corresponding cortical regions across subjects. An image analyst (R.A.D.), blind to subject diagnosis, gender, and age, traced each of 30 sulci in each hemisphere on the surface rendering of each subject's brain (13 on the medial surface, 17 on the lateral surface). On the lateral brain surface, these included the following: Sylvian fissure; central, precentral, and postcentral sulci; superior temporal sulcus (STS) main body; STS ascending branch; STS posterior branch; primary and secondary intermediate sulci; and inferior temporal, superior and inferior frontal, intraparietal, transverse occipital, olfactory, occipitotemporal, and collateral sulci. On the medial surface, these included the following: callosal sulcus, inferior callosal outline, paracentral sulcus, anterior and posterior cingulate sulci, outer segment of a double-parallel cingulate sulcus (where present) (Ono et al., 1990), superior and inferior rostral sulci, parietooccipital sulcus, anterior and posterior calcarine sulci, and subparietal sulcus. In addition to contouring the major sulci, a set of six midline landmark curves bordering the longitudinal fissure was outlined in each hemisphere to establish hemispheric gyral limits. Spatially registered grayscale image volumes in coronal, axial, and sagittal planes were available simultaneously to help disambiguate brain anatomy. Landmarks were defined according to a detailed anatomical protocol (Sowell et al., 2002a,b, 2003b) based on the Ono sulcal atlas (Ono et al., 1990). These criteria, along with inter-rater reliability measures, have been described previously (Sowell et al., 2002a,b, 2003b), and the written anatomical protocol can be obtained via the Internet (Hayashi et al., 2002). This delineation process takes an image analyst, trained in cortical neuroanatomy, ~30–45 min per brain. Before delineations are started, image analysts pass a test of inter-rater reliability that requires tracing of six brain datasets (Sowell et al., 2002a,b,

2003b), which takes several hours. Although somewhat time intensive, this process has given tracings with quantifiable reliability for large studies.

Cortical gray matter maps. Points on the cortical surfaces around and between the sulcal contours drawn on each individual's brain surface were calculated using the averaged sulcal contours as anchors to drive into correspondence the 3D cortical surface mesh models from each subject (Thompson et al., 2003). This procedure creates average 3D surface models for the WS and control groups and creates group average maps of various features of the brain surface, such as cortical thickness. In this averaging process, a cortical model with the average shape for the group is generated, and features from corresponding gyri are averaged together.

Cortical thickness. Figure 1*a–d* shows steps involved in measuring cortical thickness (Fischl and Dale, 2000; Miller et al., 2000; Jones et al., 2001; Kruggel et al., 2001; Yezzi and Prince, 2001; Annese et al., 2004). In our approach (Thompson et al., 2004), the MRI scan (Fig. 1*a*) is classified into gray matter, white matter, CSF, and a background class (represented by green, red, black, and white colors, respectively, in Fig. 1*b*). To quantify cortical gray matter thickness, we use the 3D distance measured from the cortical white/gray matter boundary in the tissue-classified brain volumes to the cortical surface (gray/CSF boundary) in each subject (Fig. 1*c*). Tissue-classified brain volumes are first resampled using trilinear interpolation to 0.33 mm isotropic voxels to obtain distance measures indexing gray matter thickness at subvoxel spatial resolution. Resampling of the tissue-segmented maps to a subvoxel spatial resolution (0.33 mm isotropic) does not provide more information than already present in the raw data, but it reduces subsequent inaccuracies in computing thickness fields by calculating distances to sets of voxels in the cortex [see Miller et al. (2000) for a related approach, in which data are interpolated to 0.5 mm before computation of distance maps]. In the resulting image, distance values are no longer forced to be computed at the sparse set of voxel locations that were in the original image. Note that the classification and upsampling steps could be done in the opposite order to retain the grayscale data as far as possible, but we found that the subsequent spatial filtering of thickness values tended to eliminate any such order effects.

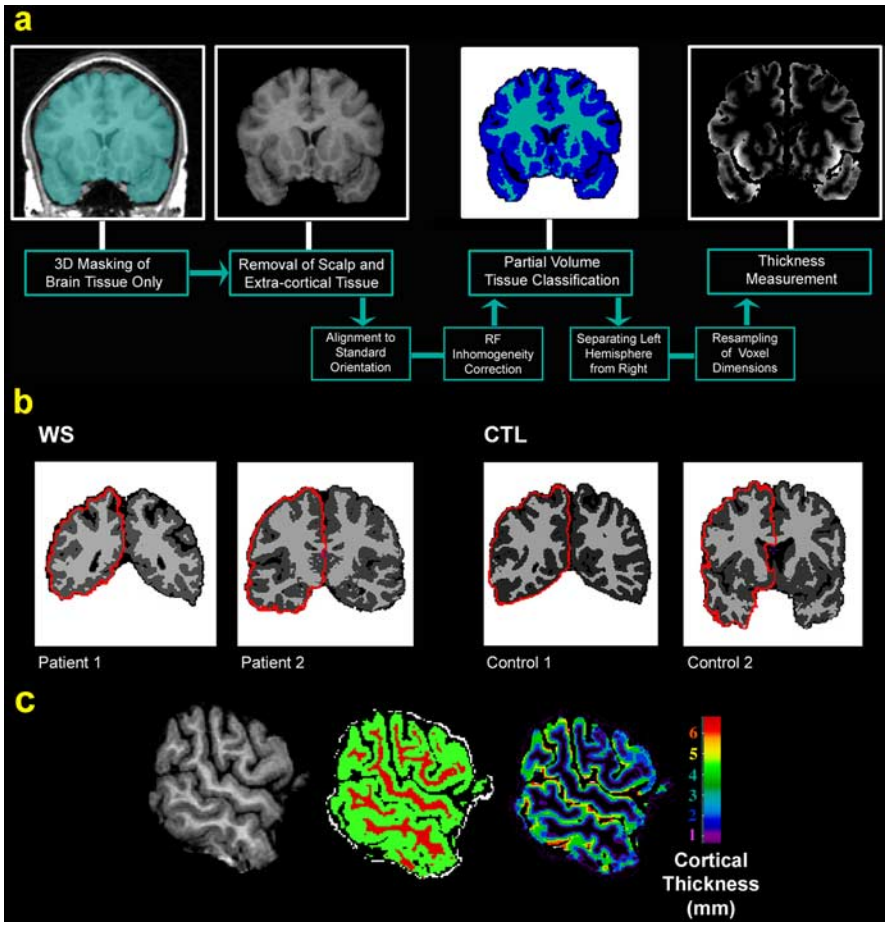

Figure 1. Steps used to create cortical thickness maps. ***a***, Sequence of steps required to derive cortical thickness maps from the MRI scans (for details, see Materials and Methods). ***b***, Representative coronal sections from the gray and white matter maps in two WS patients and two healthy controls. The extraction of a smoothed outer cortical surface is also shown in red. ***b***, ***c***, A sagittal cut from the original T1-weighted image for one representative control subject, their tissue-segmented image (***b***), and their gray matter-thickness image (***c***), in which thickness is progressively coded in millimeters from inner to outer layers of cortex using a distance field. CTL, Control; RF, radio frequency.

Gray matter thickness, measured at thousands of homologous cortical locations in each subject, was then compared across subjects and averaged at each cortical surface location, providing spatially detailed maps of local thickness differences within or between groups. The thickness data were also smoothed using a surface-based kernel of radius 10 mm to enhance signal-to-noise before making cross-subject comparisons (Memoli et al., 2004).

Modeling of gray/white matter and gray/CSF interfaces. The accurate modeling of the 3D gray/white matter and gray/CSF interfaces as well as the high-dimensional normalization of anatomy across subjects are both critical for obtaining accurate group maps of mean cortical thickness with high-enough signal-to-noise to detect regional group differences. Accuracy of the average thickness maps will be degraded by any errors in aligning the anatomy across subjects, which we counteract to some degree with cortical pattern matching and high-dimensional normalization. Also, the accuracy of the mean thickness maps will be degraded by any errors in the identification of the gray/white and gray/CSF interfaces, which we minimize by computing thickness values in the segmented image volume rather than by using the recovered 3D cortical surface. It is more convenient to digitize the entire sulcal pattern on an approximate pial surface that represents the outer (exposed) surface of the cortex and use the information to perform high-dimensional registration of anatomy across subjects. As such, we digitize the sulcal curves by tracing them as 3D parametric curves on a 3D-rendered graphical surface that represents the cortex that would be visible from the exterior of the brain [for an on-line protocol, see Hayashi et al. (2002)]. This 3D surface is obtained by optimizing a compound function that causes the surface to follow a specific intensity value in the image while reducing high-frequency noise with a term that enforces limits on the surface curvature and avoids self-intersection (MacDonald, 1998).

Even so, we ensure that the cortical thickness measures are accurate by computing them in the volume at a voxel level (they are computed from the voxel-based gray matter segmentation of the image, rather than using the vertices in the surface mesh). A similar cortical thickness-mapping approach is used by Miller et al. (2000) and Lohmann et al. (2003). This voxel-coding procedure allows faithful propagation of distance values from the gray/white interface to the gray/CSF interface. If we used the vertices of a surface mesh to compute cortical thickness, the resulting measures may be prone to inaccuracies because of departures of the vertices in the surface mesh from the exact 3D interface of gray and white matter and difficulties in following the gray/CSF interface in regions in which the sulci are narrow. As noted by Lerch et al. (2005), there are essentially two methods for computing cortical thickness: those that use a deformable surface model to compute a surface for the inner and outer gray matter surfaces (Lerch and Evans, 2004; Lerch et al., 2005) and those that use the image volume to identify gray/white matter interface and

successively propagate out distance values, using a conditional coding of voxels, until the gray/CSF interface is reached (Lohmann et al., 2003). If the first approach is used, the CSF/gray boundary is notoriously difficult to find in locations where opposing banks of cortex abut with little or no CSF between them. Instead, our approach computes thickness using the latter (voxel-coding) method. As in the studies by Miller et al. (2000), Ratnanather et al. (2001), and Lohmann et al. (2003), we identify the gray/white interface in finely resampled images (0.33 mm resolution) as the set of voxels classified as gray matter that have at least one neighboring white matter voxel, and their distance code is set to zero. In a series of subsequent passes over the image, we code successive layers of voxels that are adjacent to the voxel layer coded in the last step, and they are assigned a value equal to the closest 3D distance to the gray/white interface. The primary reason for this wavefront propagation is to prevent distances from propagating across CSF by setting the rules for serial propagation in such a way that this is forbidden. Essentially, the process computes the shortest distance from a given gray matter voxel to the nearest white matter voxel, avoiding solutions in which this line would pass through CSF. Avoidance of white matter voxels is not necessary, because the existence of a shortcut across white matter automatically implies that the shortest path has not yet been found.

This conditional voxel-coding procedure is similar to that in the study by Zhou et al. (1999), except that exact 3D distances are used to retain accuracy rather than the approximate Manhattan metric typically used in the computer graphics literature and in some fast-marching approaches for solving partial differential equations. We pass over the image repeatedly until all gray matter voxels have been assigned a distance code. This approach is advantageous because it avoids the need to find an accurate surface representation of the gray/CSF interface, which can be difficult or impossible if no CSF appears to separate gyri across the walls of a deep sulcus. If there is no detectable CSF in a deep sulcus, the current method will code gray matter voxels on either side of the sulcus with increasing distance values in a series of passes over the data until they meet in the middle. This method suffers from ambiguity when two gray matter surfaces meet without being separated by a CSF intensity voxel. In this case, the method must effectively assume that the boundary lies at the point that produces equal thickness for both of the opposing gray matter surfaces. However, this has virtually no impact on the results, because assigning one opposing surface 3 mm and the other 5 mm is effectively indistinguishable from assigning both surfaces 4 mm because of the subsequent smoothing.

Mapping distance values to the mesh surface. The sequential coding of gray matter voxels according to their 3D distance from the white matter surface results in a 3D "thickness field" within the gray matter of the cortex. Before these values can be averaged across subjects, they must be projected to the surface model. Local maxima of the 3D thickness field are retained by discarding all but a subset of voxels that fulfill either of the following criteria: (1) all gray matter voxels that are adjacent to a voxel that is nongray and nonwhite are retained; (2) all gray matter voxels with distance code that is a local maximum are retained (i.e., the distance code exceeds or equals that of all neighboring gray matter voxels; this retains gray matter voxels in deep sulci if they represent local maxima of distance). The local maxima field is then associated with the gray/CSF vertices as follows. A local smoothing kernel of radius 10 mm is defined at each vertex on the cortical surface model. The mean distance code is computed for all voxels in the local maxima field that lie under the 10 mm kernel, disregarding voxels that are not in the local maxima field. This is equivalent to applying a uniform spatial filter of a radius of 10 mm to the local maxima field, only retaining voxels with nonzero values, and reading off the resulting values at each surface vertex. Because all local maxima values are computed in the 3D volume without relying on the surface mesh, the resulting thickness map on the surface is somewhat robust to errors in the locations of surface vertices; in other words, if the surface vertices depart from the true gray/CSF interface, the net effect is to just reduce the dimensions of the spatial filter, which will not bias the value assigned to those vertices, but instead just make them more noisy. As such, the method can be seen as a hybrid approach in which a voxel-level map is used to compute thickness, but a surface mesh is used to allow high-dimensional normalization of these values across subjects.

Validity and reproducibility of the cortical thickness measure. Given that laminar structure is not visible with MRI, we could not rely on laminar structure to define cortical thickness, as we have done using other automated approaches in histological data (Annese et al., 2004). The regional variations in these maps agree with those found in the classical cortical thickness maps derived postmortem by von Economo and have been shown to be stable over time in validation studies using short-interval repeat scanning of multiple subjects (Sowell et al., 2004). In that study, we analyzed longitudinal scans on three healthy young adults at short intervals (two subjects were scanned twice, and one subject was scanned three times, 3 weeks apart; we estimated individual rescan reliability for cortical thickness, combined over many subjects, and this revealed a maximum error in the group average cortical thickness of 0.15 mm with errors much less in most areas). Even this maximum error in the group average cortical thickness is considerably lower than the group differences observed in the sample. In the study by Narr et al. (2005), we replicated this profile of mean cortical thickness by applying the same method in an independent sample of $n = 78$ healthy subjects who were controls in a study of 72 first-episode schizophrenia patients.

Given the large anatomical variability in some cortical regions, high-dimensional elastic matching of cortical patterns (Thompson et al., 2004) was used to associate measures of cortical gray matter thickness from homologous cortical regions across subjects. One advantage of cortical matching is that it localizes deficits relative to gyral landmarks; it also averages data from corresponding gyri, which would be impossible if data were only linearly mapped into stereotaxic space.

Choice of smoothing filter. In this study, the thickness maps were spatially filtered for three reasons. First, smoothing reduces high-frequency noise in the cortical thickness measures. Because the cortex is only ~3–6 voxels thick in the original MRI data, noise in the thickness estimates can be reduced by replacing individual vertex values with neighborhood averages, increasing the spatial coherence of the thickness values (cf. Lerch and Evans, 2005). Second, by the central limit theorem, filtering increases the normality of the residuals after a statistical model is fitted and improves the power of the statistical tests (although their validity is guaranteed here by permutation testing). Finally, smoothing reduces the effects of imperfect alignment of anatomy. In voxel-based morphometry, typically only simple, low-order, anatomical normalization is performed, and thus relatively large smoothing filters are needed to reduce effects of anatomical misregistration [for a comparison of smoothing filters, see Salmond et al. (2002)]. In contrast, cortical pattern matching greatly reduces cross-subject misregistration of anatomy, reducing the need for a broad smoothing filter. This is advantageous, because minimal smoothing sensitizes the analysis to regional differences at a small spatial scale. By the matched filter theorem, the optimal filter size should reflect the scale of the signal being detected. Because we expected to find differences at approximately the scale of a gyrus (~10 mm) or in larger regions, we used a 10 mm smoothing kernel. A recent validation study of cortical thickness by Lerch and Evans (2005) found that sensitivity was optimal with a 30 mm blurring kernel, although they did not apply cortical pattern matching to align corresponding anatomy across subjects. Studies are underway to define the optimal filtering method, including using level-set implementations (Memoli et al., 2004), although this depends on the scale of the expected signal and accordingly varies somewhat for each application.

Statistical maps of cortical thickness. Statistical maps were generated, indicating group differences in local gray matter thickness. To do this, at each cortical point, a regression was run to assess whether the thickness of the cortical gray matter at that point depended on group membership. The p value describing the significance of this linkage was plotted at each point on the cortex using a color code to produce a statistical map. The statistical maps (uncorrected) are crucial to visualize the spatial patterns of gray matter deficits, but permutation methods (Bullmore et al., 1999; Thompson et al., 2003) were used to assess the significance of the statistical maps and to correct for multiple comparisons. In each case, the covariate (group membership) was permuted 1,000,000 times on a Silicon Graphics (Mountain View, CA) Reality Monster supercomputer with 32 internal R10000 processors, and a null distribution was developed for the area of the average cortex with group-difference statistics

above a fixed threshold in the significance maps. An algorithm was then developed to report the significance probability for the overall group differences in each map as a whole (Thompson et al., 2003) after the appropriate correction for multiple comparisons.

Cortical complexity. We also developed an algorithm to measure the fractal dimension, or complexity, of the human cerebral cortex, based on a previous algorithm that we developed for mapping the complexity of deep sulcal surfaces in the brain (Thompson et al., 1996). The steps are shown in Figure 2. Previous approaches for measuring gyrification have typically compared the length of an inner and outer cortical contour in 2D slices of the brain (Fig. 2*a*) (adapted from Zilles et al., 1988) (Bartley et al., 1997; Kulynych et al., 1997; Vogeley et al., 2000). A gyrification index (GI) can be computed expressing how much the length of the deep cortical contours exceeds the length of a hypothetical convex outer contour enclosing the brain. Unfortunately, this measured value will vary depending on the direction in which the brain is sliced; thus, it is biased by the orientation of slicing the brain (specifically, it is more sensitive to folding in gyri running orthogonal to the plane of section, less sensitive to folding parallel to the plane of section, and differentially sensitive to folding in gyri with intermediate orientations). Instead, we computed fractal dimension of the cortex in three dimensions by using the surface mesh that represents the cortex (Fig. 2*b*). This takes into account the full 3D surface geometry, and the resulting measure is independent of brain size and orientation and does not depend on the direction of image acquisition. As with other gyrification measures, this fractal measure does not depend on the scale of the brain (because it is essentially a ratio). In our approach, a cortical pattern-matching step can be used to adapt surface meshes precisely to lobar subregions using anatomical constraints. This allows complexity to be measured for precisely defined lobar surfaces defined individually in each subject.

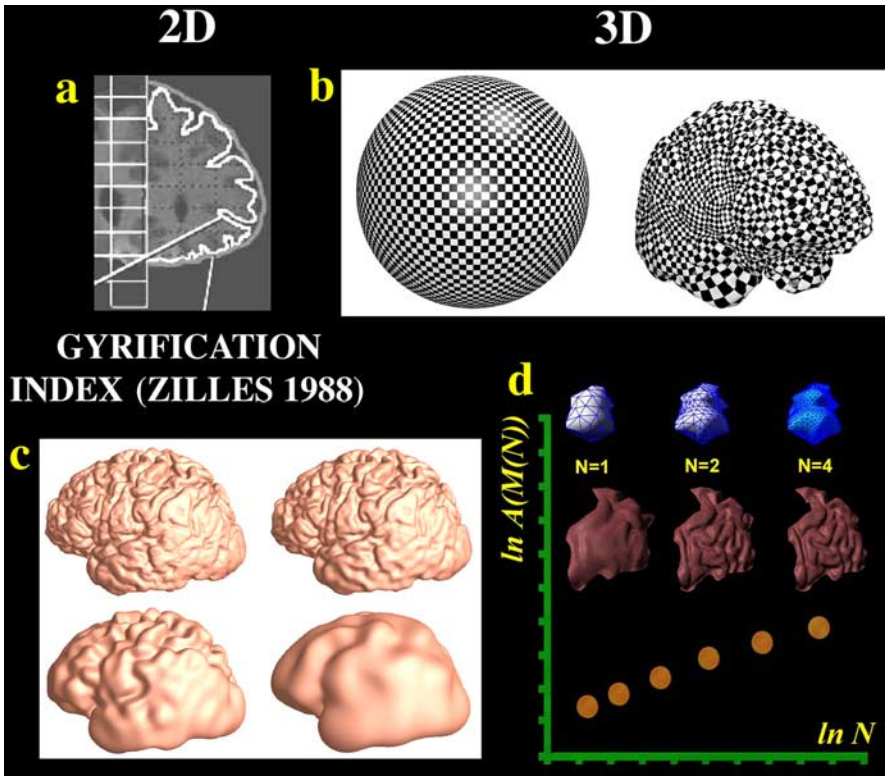

Figure 2. Measuring cortical complexity in three dimensions. Measuring cortical complexity in three dimensions avoids biases with GIs that depend on the orientation in which the brain is sliced. ***a***, The idea behind gyrification indices, which measure cortical folding based on a series of MRI sections [adapted from Zilles et al. (1988)]. The GI compares the perimeter of the inner contour of the cortex, following sulcal crevices, with the perimeter of the cortical convex hull, which is the convex curve with smallest area that encloses the cortex. The ratio of these is computed and expressed as a weighted mean across slices. Instead, our approach computes complexity from a spherical surface mesh that is deformed onto the cortex (***b***). The cortex is then mathematically regridded at successively decreasing frequencies (***c***), such that smoother cortices have less surface area. By plotting the observed surface area versus the cutoff spatial frequency in the surface representation, on a log–log plot (***d***), more complex objects have greater gradients. This plot is called a multifractal plot: the *x*-axis represents the log of number of nodes in the surface grid (here denoted by ln *N*), and the *y*-axis measures the log of the surface area of the resulting mesh [here denoted by ln $A(M(N))$, where A is the area function and $M(N)$ is the surface mesh with N nodes]. For nonflat surfaces, this plot has a positive slope, because the surface area increases as more nodes are included in the mesh. The slope of this plot is added to 2 to get the fractal dimension of the surface (Thompson et al., 1996) [***b*** and ***c*** were adapted from Gu et al. (2003)]. Adding the gradient of the multifractal plot to 2 is a convention used when computing fractal dimensions for surfaces. It ensures that the computed fractal dimension of a flat 2D plane agrees with its Euclidean dimension, which is 2, because the surface is 2D (for details, see Materials and Methods).

To compute complexity, the cortical pattern-matching technique uses sulcal landmarks as anchors to reparameterize the cortex so that corresponding sulci and cortical regions occur at the same parameter space locations (Thompson et al., 2004). The resulting deformed spherical parameterization is discretized in parameter space, using a hierarchy of quadtree meshes of size $n \times n$, for $n = 2$ to 256. The cortex is remeshed at each spatial frequency (Fig. 2*c*), and its surface area is measured. The rate of increase of surface area with increasing spatial frequency is estimated by least-squares fitting of a linear model to the estimated surface area versus frequency, on a log–log plot (Fig. 2*d*) [this plot is termed a multifractal plot in the fractal literature; for a discussion of this concept, see Kiselev et al. (2003)]. If $A\{M(N)\}$ represents the surface area of the cortical surface mesh $M(N)$, the fractal dimension or complexity is computed as $\mathrm{Dim}_F = 2 + \{d(A\{M(N)\})/d \ln N\}$. The gradient of the multifractal plot is obtained by regressing $\ln A\{M(N)\}$ against $\ln N$. For a flat surface, this slope is zero, and the dimension is 2; representing the surface at a higher spatial frequency adds no detail. Values >2 indicate increasing surface detail and greater gyral complexity. Intuitively, higher complexity means that the area increases rapidly as finer scale details are included. We applied this algorithm to study gender differences in cortical complexity in healthy adults (Luders et al., 2004).

By computing surface complexity from 3D meshes, two weaknesses of previous gyrification indices are avoided. First, the surface-based fractal measure is independent of the direction in which the brain is sliced, which affects gyrification measures based on sampled cross sections. This bias can be appreciated by noting that a corrugated 3D surface may appear to have a sinusoidal or completely linear cross section, depending on which direction it is cut [for a presentation and discussion of this problem, see Barth et al. (1993)]. The second advantage of measuring complexity from surface meshes is that they can be adapted precisely to individual lobar anatomy. To do this, a cortical pattern-matching procedure uses carefully defined sulcal landmarks that delimit the lobes in each subject. Homologous brain regions are then compared across subjects and groups to the highest possible degree. If a stereotaxic template is used to parcellate the brain into regions, it will not in general label the same anatomy because of wide individual variations. This differential labeling makes any observed differences difficult to interpret.

Results

Overall volumetric differences

To provide context for the cortical thickness maps, the overall reductions in total gray and white matter in WS are shown in Figure 3. First, agreeing with previous volumetric studies using different tissue classification and analysis methods (Reiss et al., 2004), the WS group had greatly reduced overall brain volumes (by 12.7%; $p < 0.0001$; left and right hemisphere volumes were

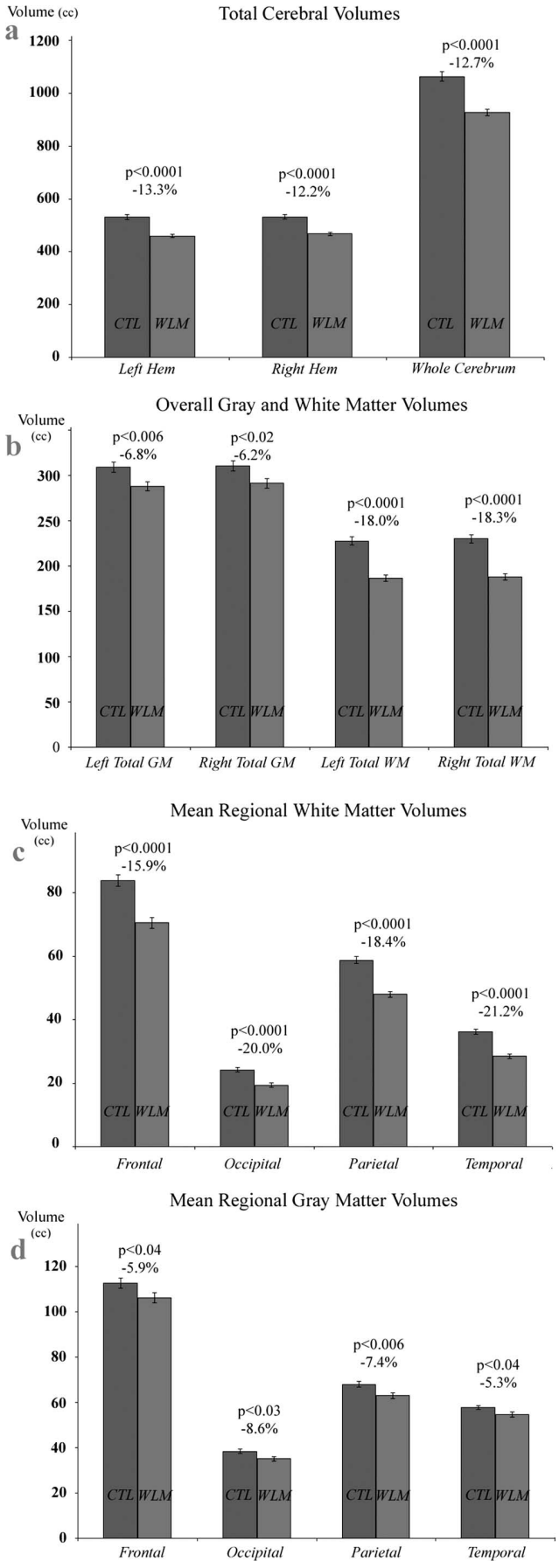

reduced by 13.3 and 12.2%, respectively) (Fig. 3*a*). Second, this overall deficit was attributable to primarily a far more dramatic reduction in white matter (left hemisphere, −18.0%, $p < 0.0001$; right hemisphere, −18.3%, $p < 0.0001$) than gray matter, although gray matter also was reduced severely (left hemisphere, −6.8%, $p < 0.006$; right hemisphere, −6.2%, $p < 0.02$). At the lobar level, the WM deficit was found somewhat uniformly across all lobes (frontal, −15.9%; parietal, −18.4%; temporal, −21.2%; occipital, −20.0%; all $p < 0.0001$) (Fig. 3*c*). Lobar GM volumes also appeared uniformly reduced (frontal, −5.9%; parietal, −7.4%; temporal, −5.3%; occipital, −8.6%; all $p < 0.04$) (Fig. 3*d*). However, although these overall measures give an impression that the GM deficit is uniform across the brain, this is not the case, as shown by the cortical thickness maps.

Cortical thickness maps

Average maps of cortical thickness are shown for the WS and control groups in Figure 4, *a* and *b*. The WS group had greatly increased cortical thickness in a large neuroanatomical region encompassing the perisylvian language-related cortex. This region surrounds the posterior limit of the Sylvian fissures and extends inferiorly into the lateral temporal lobes (Figure 4*c*, red colors denote a 10% thickening of the cortex relative to controls). The region of significant thickness increases also extended over the inferior surface of the right temporal lobe (Fig. 4*e*) into the collateral and entorhinal cortex. This region included the fusiform face area, which processes facial stimuli, a cognitive ability in which WS subjects show notable strengths. We also compared the mean difference in thickness with a pointwise estimate of the SE in cortical thickness to measure the significance of the thickness increases. This significance map is shown in Figure 4*d*. Correcting for multiple comparisons, the right hemisphere thickness increase was highly significant ($p < 0.002$), but the apparent left hemisphere increase was not significant ($p = 0.27$). To better evaluate the anatomical selectivity of the effect, Figure 4*c* shows that the mean increase in cortical thickness was detected in the right hemisphere only. It remains possible that there is some regional thickening in the left hemisphere, but a very large sample may be needed to detect it, if present. There may be low power to detect a subtle reduction in cortical thickness in the same left hemisphere systems, especially when correcting for multiple comparisons across the whole hemispheric surface.

Adjacent GM deficits

Regions with lower mean cortical thickness in WS are shown in Figure 5; these include large contiguous regions of cortex in

←

Figure 3. Comparison of brain structure volumes in Williams syndrome and healthy controls. ***a–d***, Means and SE measures (error bars) are shown for the volumes of the cerebral hemispheres (***a***), overall cerebral gray and white matter (***b***), lobar white matter (***c***), and lobar gray matter (***d***). WS subjects show significant gray and white matter reductions in all lobes, but the brain volume reduction is mainly attributable to white matter deficits. Involvement of all lobes is compatible with the notion that in all lobes, subcortical white matter carries long projections not necessarily related to the lobe in which it is found (e.g., the parietal white matter contains fibers connecting occipital and frontal lobes). Previous anatomical parcellations suggested disproportionately smaller occipital lobes and larger orbitofrontal and superior temporal gyri (Reiss et al., 2004), whereas the corpus callosum (Schmitt et al., 2001) and cerebellum (Jernigan et al., 1993) were relatively preserved. Cortical maps now reveal the profile of thickness increases and decreases over the entire cortex and support previous findings of increased gray matter density bilaterally in the fusiform and middle temporal gyri and insula (Reiss et al., 2004). CTL, Control; Hem, hemisphere; WLM, Williams syndrome.

each of the lobes, including components of the lateral surface that surround the interhemispheric margin and most of the medial wall.

Increased cortical complexity

Cortical complexity was also significantly increased in WS for both brain hemispheres (Fig. 6). Left hemisphere complexity in the Williams group (2.2522 ± 0.0016 SE) was greater than that in controls (2.2457 ± 0.0014; $p < 0.00145$; two-tailed t test). Right hemisphere complexity was also increased (2.2522 ± 0.0016 SE in WS, compared with 2.2490 ± 0.0016 in controls; $p < 0.0014$; two-tailed t test). Differences were significant with or without adjusting for effects of age and gender. Although these differences appear to be small in magnitude (~0.1–0.3%), this can be misleading because they are computed from a log–log plot, in which small differences in slope translate into very large differences in gyral complexity.

Steinmetz classification

To better understand the increased complexity in terms of accepted neuroanatomical criteria, we attempted to identify specific gyral alterations that might be associated with diagnosis using criteria defined by Steinmetz (1996). We found that in 66 subjects, the right Sylvian fissure ascended behind the postcentral sulcus (type I, according to the Steinmetz classification) (Steinmetz, 1996), while the Sylvian fissure merged with the postcentral sulcus in five subjects (Steinmetz classification, type IV). In an additional 11 WS subjects, the right Sylvian fissure ascended behind the sulcus of Jensen (i.e., at least three sulci, including the central sulcus, were anterior to the Sylvian fissure; type III), whereas none of the controls exhibited the type III morphology in the right hemisphere ($\chi^2 = 12.67$; $p < 0.005$). There was no difference in the frequency of types II or III morphology in the left hemisphere (type II means the Sylvian fissure fails to ascend into the parietal lobe and remains horizontal). This was expected, given the relatively high frequency of types II and III morphology in normal left hemispheres. Although there was no difference in hemispheric complexity between the Steinmetz classification types in the WS right hemisphere ($F_{(1,39)} = 0.24$; NS), WS subjects with the right hemisphere type III morphology had a significantly more complex left hemisphere than WS subjects with the right hemisphere type I morphology ($F_{(1,39)} = 7.43$; $p < 0.01$). In addition, many WS brains exhibited increased fissuration in the central-postcentral regions (Fig. 7); this may have contributed to the anomalous increases in complexity observed in the WS group and found in both brain hemispheres.

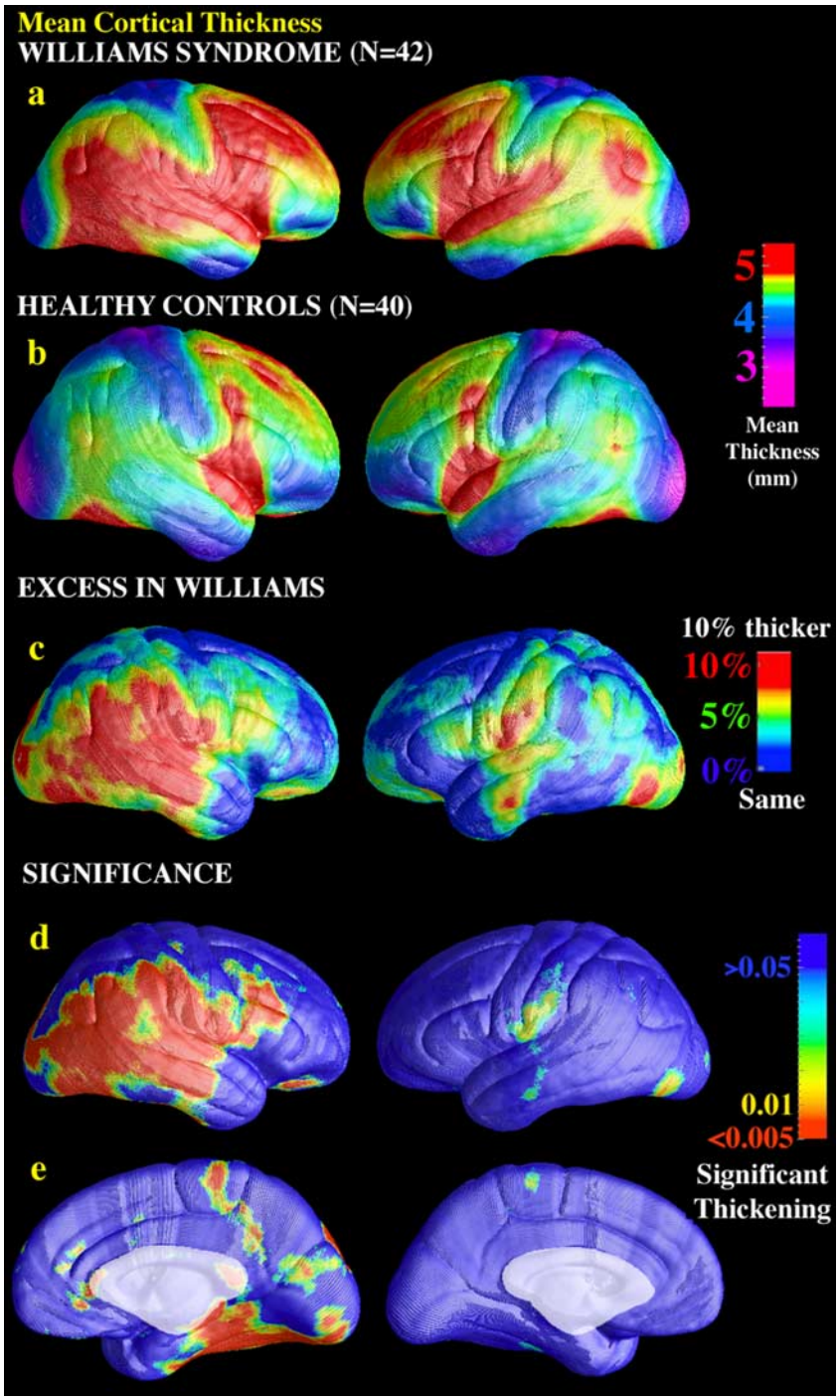

Figure 4. Cortical thickness maps: regional increases in WS. The mean cortical thickness for WS subjects (***a***) ($n = 42$) and controls (***b***) ($n = 40$) is shown on a color-coded scale, in which red colors denote a thicker cortex and blue colors denote a thinner cortex. Thickness is measured in millimeters, according to the color bar. The mean increase in cortical thickness in WS is shown as a percentage of the control average in ***c***. Red colors in perisylvian cortices denote regions that are up to 10% thicker, on average, than corresponding areas in controls. The significance of these changes on the lateral surface (***d***) and medial surface (***e***) of each brain hemisphere is shown. ***e*** shows that the right inferior temporal cortex is thicker in WS. Thickness increases in the left hemisphere were not significant after correcting for multiple comparisons. Although some right-sided cortical regions have increased cortical thickness, this may not reflect greater gray matter volume in discrete cortical areas. Thickness may increase in areas with reduced surface extent; the cortex may thicken if comparable numbers of cortical cells crowd over a white matter volume with reduced surface extent. The abnormally thick cortex may therefore be abnormally functioning cortex.

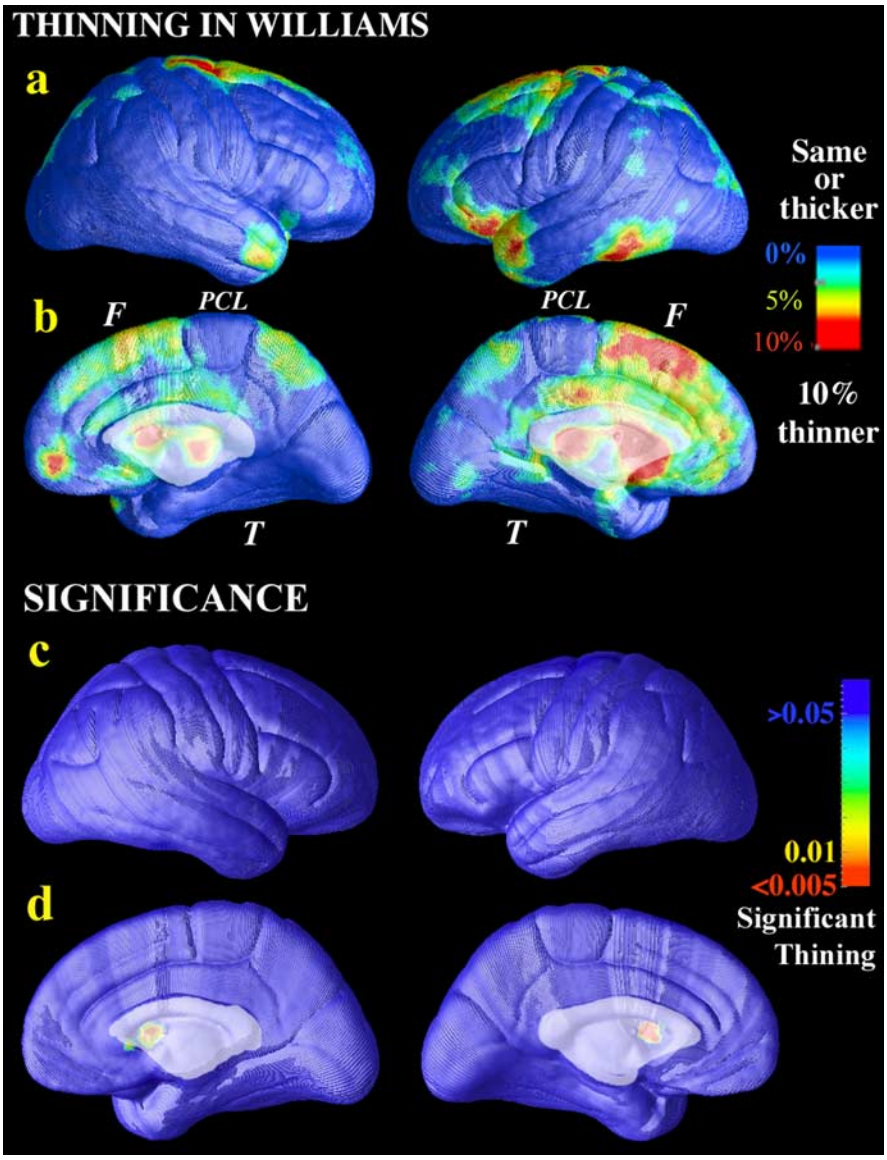

Figure 5. Cortical thickness maps: regional decreases in WS. In some regions of the dorsal stream, the estimated mean cortical thickness in WS was lower than the mean value in controls (***a***, ***b***), but these reductions were not found to be significant (***c***, ***d***) after permutation testing, which corrects for multiple comparisons. This failure of thinning to reach significance may relate to the variance in the measures of cortical thickness (Fig. 9*c*,*d*), which may be lower in histology than in MRI-based measures (in which few voxels span the cortex). Red colors in ***a*** and ***b*** denote brain regions in which mean cortical thickness was ~10% lower than the control mean. Blue colors denote regions in which the thickness was the same or higher in WS. A recent finding of reduced superior parietal lobule volume in WS, even after adjusting for differences in brain volume (Eckert et al., 2005), is consistent with the medial superior parietal reductions seen here. F and T denote frontal and temporal cortices, respectively, and PCL denotes the paracentral lobule. Even so, postmortem architectonic measurements are not straightforwardly related to MRI findings in WS. In the visual cortex, smaller cells and increased packing have been found in the left hemisphere. This might predict thinner cortex on MRI. Occipital gray matter volumes were reduced on MRI, but the diffuse reduction in cortical thickness was not significant here after multiple-comparisons correction.

Complexity is correlated with cortical thickness

To determine whether greater cortical thickness was associated with higher cortical complexity, we created maps correlating the two features (Fig. 8). At each cortical location, the thickness at that location was regressed against the overall complexity value for the brain hemisphere. In normal subjects ($n = 40$), increased complexity was highly correlated with thicker cortex in the right hemisphere ($p < 0.03$). The relationship between cortical thickness and complexity was weaker in the left hemisphere (showing only weak effects in perisylvian and central regions) and not significant after multiple-comparisons correction ($p = 0.18$). Only weaker links between cortical thickness and complexity were found for the WS subjects (data not shown; maps were not significant after multiple comparisons). Healthy subjects with higher cortical complexity had thicker cortex in a broad right hemisphere region that included perisylvian, primary sensorimotor, occipital, and cingulate regions (Fig. 8). Cortical complexity and thickness were not associated in the left hemisphere in normal subjects or in either hemisphere for WS subjects; although WS subjects had overall greater complexity, they had less gray matter and thinner cortices overall. If cortical thickness and complexity were positively correlated in general, the frontal and parietal regions of greater gyrification found by Schmitt et al. (2002) would be expected to show greater cortical thickness, but this was not found. No simple universal relationship was therefore found between thickness and complexity, and careful study of these measures in larger samples is warranted.

Age effects on cortical thickness

Figure 9, *a* and *b*, shows maps of age effects on cortical thickness. After multiple-comparisons correction, age-related thinning was significant in the left hemisphere but not the right hemisphere ($p = 0.02$ and 0.09, respectively). Age effects were not detected in the perisylvian regions where thickening was observed in patients. In our previous study (Sowell et al., 2003a), quadratic effects of age were significant over the entire cortex, but here they were detected only in some regions, because they are subtle and the sample and age range are smaller [relative to the 176 subjects 7–87 years of age in the study by Sowell et al. (2003a)]. Figure 9, *c* and *d*, shows the SD in cortical thickness in the healthy controls (maps for WS subjects were similar). Red colors indicate that normal variability in cortical thickness is highest in perisylvian areas.

Discussion

Three key findings of this study reveal cortical anomalies associated with the genetic deletion in Williams syndrome. Cortical thickness was significantly increased (by 5–10%) in a broad anatomical region, encompassing perisylvian regions important for language comprehension. These regions, especially in the right hemisphere, process linguistic and musical syntax and prosody (Ross and Mesulam, 1979; Cabeza and Nyberg, 2000), areas in which WS subjects have relative strengths. Against the backdrop of widespread brain

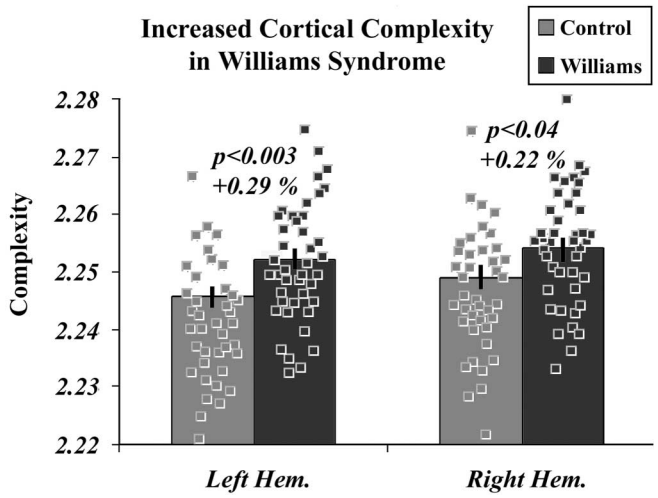

Figure 6. Cortical complexity is increased in WS. The mean cortical complexity and SEs are shown for controls and for WS subjects. Black and gray squares denote data points from individual subjects in the study. In WS, cortical surface complexity is increased in both brain hemispheres. This extends previous work measuring gyrification in 2D serial sections (Schmitt et al., 2002). Postmortem studies have found multiple small gyri in dorsal cortical regions (Galaburda and Bellugi, 2000), and increased fissuration is often apparent in the WS brain by visual inspection (Fig. 7). Schmitt et al. (2002) examined gyrification patterns in 17 WS subjects and 17 controls and found significantly increased cortical gyrification globally, with greater abnormalities in right parietal ($p = 0.02$), right occipital ($p = 0.02$), and left frontal ($p = 0.009$) regions. These regional gyrification effects (such as the increased folding shown in Fig. 7) are not so easily localized using a global measure such as fractal dimension. Hem., Hemisphere.

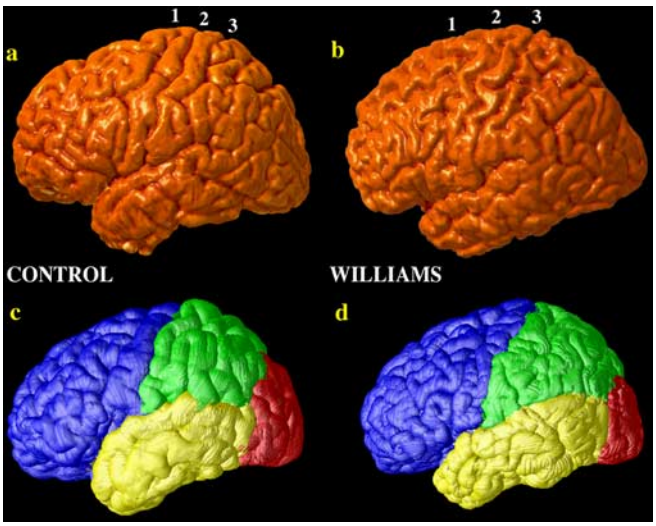

Figure 7. Gyrification differences in WS. The fissuration pattern of the precentral, central, and postcentral sulci (labeled 1, 2, and 3, respectively) is typically very simple in control subjects but more complex in WS. A typical control subject (***a***) and a typical WS subject (***b***) are shown. Note the thinner gyri in the WS subject and increased fissuration in the paracentral area. ***c*** and ***d*** show how the surface mesh models of the cortex were partitioned into lobes for a normal subject (***c***) and a WS subject (***d***). Cortical pattern matching allows corresponding regions of parameter space to index the same anatomy across subjects, allowing accurate partitioning of anatomy. The cortical registration approach used here identifies the maximal subset of sulci that occur consistently in all subjects, and these are used to align anatomy across subjects. These sulci are always present in the WS subjects as well as in controls. Even so, in individual subjects, there may be additional accessory sulci or fissures created by abnormal folding (as seen here). These sulci are not used in the anatomical normalization (because they do not have counterparts in all other brains); they are therefore situated between the major cortical sulci that are aligned.

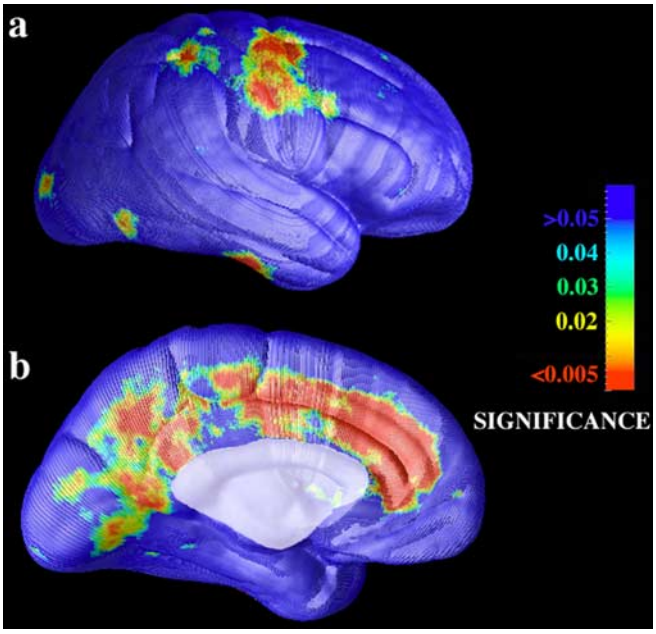

Figure 8. Cortical thickness and complexity are correlated. Lateral (***a***) and medial (***b***) views of the cortex are shown. In healthy normal subjects ($n = 40$), higher cortical complexity is correlated with thicker cortex in right perisylvian areas, primary sensorimotor and visual cortices, and a broad band of cingulate/paracingulate cortex ($p < 0.02$). At each cortical location, the thickness at that location was regressed against the overall complexity value for the brain hemisphere. Regions in which there is a significant linkage between cortical thickness and hemispheric complexity are shown. No relationships were detected in the left hemisphere or in the WS subjects for either hemisphere. Our ongoing mathematical work will recast the fractal dimension as the surface integral of a fractal density measure, which is more likely to correlate pointwise with cortical thickness than global complexity measures. Such work may make it possible to compute the fractal dimension directly from the curvature tensor and metric of the cortical surface. Across species, the cerebral gray/white matter ratio obeys an allometric power law that predicts increased gray matter fissuration as brain size increases (Zhang and Sejnowski, 2000). It is unknown whether a similar power law is found within species; we recently found that mean cortical complexity was higher in women than in men (Luders et al., 2004), and women generally have a higher proportion of gray matter (relative to total brain volume) than men, consistent with a hypothetical relationship between cortical thickness and complexity.

tissue deficits, the perisylvian cortex was thicker in WS than in controls.

Functional interpretation

One simplistic interpretation is that thicker cortex is better, and that regionally thicker language cortex in WS subjects may account for their verbal strengths and unusually expressive language. By a similar argument, WS subjects are also prone to seek the gaze of others (Mervis et al., 2003), and the thicker cortical region in WS also encompasses the superior temporal sulcus, an area important in face and gaze processing (Kanwisher et al., 1997; Zeineh et al., 2003). However, this interpretation is unduly simplistic for several reasons. First, WS subjects have relatively intact language, but they do not outperform controls, which would be implied by the idea that thicker cortex is better (Haier et al., 2004). Second, WS subjects do not have enhanced function in other systems with thicker cortex (e.g., posterior and lateral occipital and inferior occipital-temporal regions), which subserve visuospatial functions impaired in WS. Third, a similar thickening of perisylvian cortex in fetal alcohol syndrome (FAS) (Sowell et al., 2002b) is not associated with better language function. In cognitive-processing models (Kosslyn, 1994), larger processing networks with more processing units are advantageous in some cases, whereas in other cases, smaller ones are optimal. In some

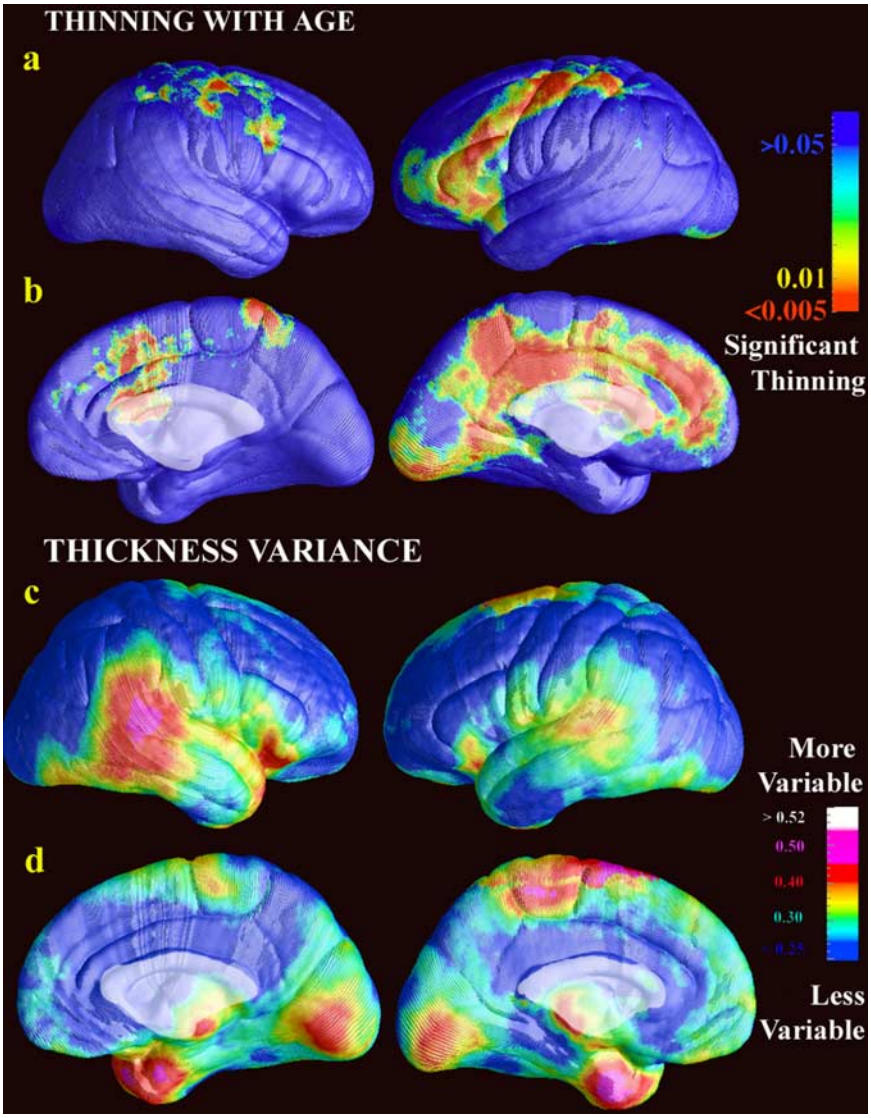

Figure 9. Age effects and variation in cortical thickness. ***a***, ***b***, Brain regions in which significant cortical thinning with increasing age was detected (red colors). ***c***, ***d***, The SD in cortical thickness in the 40 controls at each point of cortex, showing the high variance in the perisylvian cortex. Maps were similar in WS (not shown in this figure). The statistical power for detecting group differences in cortical thickness is spatially variable and depends on the 3D anatomical variability of each region across subjects after data are aligned to a common space as well as the local intersubject variance in cortical thickness (***c***, ***d***). High-anatomical variability typically reduces statistical power for detecting group differences (because of confounding anatomical noise). The posterior limits of the Sylvian fissures and surrounding perisylvian territory have extremely high variability (~15–20 mm 3D rms variability in Talairach stereotaxic space) in part because of the wide variations in the termination points of the ascending and posterior branches of the Sylvian fissures and superior temporal sulci (Thompson et al., 2000, 2001a). Without efforts to overcome this variability, such as the high-dimensional anatomical normalization used in this study, there is an intrinsically lower power for finding gray matter differences in the perisylvian region, relative to other brain regions (Witelson and Kigar, 1992). This is likely why gray matter differences were not found in these regions using voxel-based morphometry (Reiss et al., 2004), because only a low-order anatomical normalization was used. A cortical pattern-matching approach is used in this study to overcome this high variability, explicitly using sulcal landmarks to align cortical regions and increase the homology of anatomical comparisons and the resulting signal-to-noise ratio. As observed in the statistical maps, there was sufficient power to detect group differences in cortical thickness in the perisylvian areas, despite their very high anatomical variability.

cases, thinner cortex may reflect more efficient neural packing, as has been suggested to explain gender differences in regional cortical volumes. Cortical alterations in either direction (thickening or thinning) may reflect deficiencies, but either of these changes, or both, may reflect attempts to compensate. Whether or not they succeed requires additional testing.

Second, the cortical thickening is remarkable given the dramatic overall tissue reductions in WS. Consistent with previous findings using independent methods (Reiss et al., 2004), the overall brain volume deficit in WS is ~13% (Fig. 3). This deficit is primarily because of a 15–21% white matter reduction in all lobes, compared with a 6–8% gray matter reduction, which is also significant in all lobes. Despite this, the perisylvian cortex is thicker than adjacent dorsal stream regions (including parietooccipital areas with volume reductions and impaired functional activations) (Meyer-Lindenberg et al., 2004; Eckert et al., 2005). The map of cortical thickness reductions helps to explain why GM volume can be significantly reduced overall in every lobe, even when the cortex is thicker in a perisylvian region that impinges on all lobes. In all the major lobes, significantly thickened cortex lies adjacent to brain regions with significant GM loss. These findings may therefore be missed in volumetric studies but are readily identified by thickness maps.

Possible mechanisms

Perisylvian cortical thickening may result from a selective failure of these systems to myelinate, which could result in more tissue segmenting as gray matter in these brain regions. However, this explanation is unlikely in WS, because a failure to myelinate would likely promote severe deficits rather than relative strengths in the functions these regions subserve, and the thinner regions subserve impaired functions (e.g., visuospatial skills), whereas thicker regions subserve relatively strong functions (language and face processing). Intriguingly, as observed here in WS, subjects with FAS exhibit a selective 15% increase in gray matter density in the perisylvian and inferior parietal cortices bilaterally ($p < 0.001$, left and right hemispheres) (Sowell et al., 2002b). The WS genetic lesion may be sufficient, but not necessary, to induce selective anomalies in perisylvian cortex, and the same systems may be especially vulnerable to alcohol neurotoxicity during cortical maturation.

In both WS and FAS, excess cortical gray matter is most likely a result of a failure of cortical formation during gyrogenesis or a concomitant failure or delay in myelination, perhaps specifically in subcortical U-fibers (conventional MRI cannot distinguish these two possibilities). The gray/white matter junction is sharper in sulcal beds than in gyral crests, in which the deeper layers "taper off" into the white matter. With increased cortical complexity (i.e., more gyri), the gray/white junction may become more indistinct as neurons taper off into the white matter, not because of decreased myelination. Also, gray matter loss is observed consistently with longitudinal MRI in late childhood and adolescence (Jernigan et al., 2001;

Gogtay et al., 2004; Sowell et al., 2004). This loss is usually attributed to neuropil pruning seen histologically. If thickness increases reflect delayed or failed pruning of neuropil, their cellular basis may be clarified using *N*-acetylaspartate MR spectroscopy or intracortical diffusion tensor imaging to assess neuronal markers and cellular architecture in these cortical regions. Diffusion MRI and spectroscopic techniques now lack the anatomical resolution to resolve these issues, but their detection sensitivity could be improved if focused on the regions identified here. Although the current study focused on gray matter thickness, the volumetric deficits were proportionally more severe in white matter (~18% deficit) than in gray matter (~7%). Complementary studies are required using relaxometry (e.g., parametric imaging) (Bartzokis et al., 2004), spectroscopy, and diffusion tensor imaging to create composite maps of white matter parameters as well as cortical activation studies to assess its functional integrity (Meyer-Lindeberg et al., 2004).

Cortical architecture in WS is likely influenced by haploinsufficiency for specific deleted genes, but it is also dynamic and environmentally influenced throughout life. This study correlates genetic mutation and anatomical change, but causality cannot be determined. There is no way to make any simple categorical interpretation of genetic and nongenetic influences, because these cannot be disentangled, and both may occur downstream of a genetic lesion. The observed cortical thinning may be shaped primarily by negative genetic influences (that impair parietal-occipital structure and function). Nonetheless, the cortical increases may represent increased use or overuse of specific networks. Even if the thickening represents an adaptive response to the genetic deletion, whether or not it is functionally advantageous cannot be assessed without additional testing. Conversely, a cortex that appears relatively intact on MRI is not necessarily functionally intact. The notion that there are functions left intact in developmental disorders is likely incorrect; massive reorganization is likely standard across developmental disorders, and the resultant functionality is probably deviant (Karmiloff-Smith et al., 1997; Mills et al., 2000; Thomas and Karmiloff-Smith, 2002; Grice et al., 2003). In particular, language processing, musical abilities, and face processing in WS are not par with normal performance (Karmiloff-Smith et al., 1998, 2004). Prospective-longitudinal studies of very young children with WS may elucidate developmental factors contributing to altered neurodevelopment.

Cellular correlates

In both WS and healthy subjects, the perisylvian cortex is thicker than the surrounding cortex, and WS subjects have an absolute increase in perisylvian cortical thickness compared with controls. In Holinger et al. (2005), we found larger cells in the primary auditory area, Heschl's gyrus, a finding congruent with the cortical thickening seen here. An areal expansion of the thicker perisylvian region would be easier to explain, because the cortex covering the reduced white matter would have to thicken to fit the smaller volume on physical grounds only. If WS subjects have disproportionately reduced white matter, cortical cells fitting over a smaller white matter area may pile up, and the cortex may thicken because of a crowding effect. Histologic studies in WS have found a tendency for larger neurons in layer III of area 41 but no overall differences in cell size or packing density (Holinger et al., 2005). Decreased underlying white matter may cause tangential compression and neuronal crowding in WS and more neurons in a radial distribution, although there is little normal variation in the number of neurons comprising a radial column (Rockel et al., 1974).

Future work on the molecular genetics of WS may reveal whether increased gyrification is a consequence of the cortical thickening. Differential laminar growth or mechanical/tensile factors in the underlying axons may increase cortical complexity (Richman et al., 1975; Van Essen, 1997). Alternatively, the deleted genes may directly contribute to fissuration in the normal human cortex. Some *Wnt* signaling genes, which direct early cell differentiation and segmentation, are housed in the deleted 7q11.23 chromosomal region in WS (Cadigan and Nusse, 1997), suggesting a possible genetic basis for the cortical dysmorphology observed here.

Neuroanatomical descriptors of WS are important to identify to better understand the symptoms, cognitive sequelas, and potential for therapy in patients with WS. The 7q11.23 WS genetic deletion is known, and cortical systems have now been identified, the maturation of which it affects. As the time course of perisylvian gyrogenesis and maturation is increasingly understood (Gogtay et al., 2004), the timing of the cortical anomaly in WS and the genetic cascades and gene-environment interactions that underlie it will be more completely established.

References

Annese J, Pitiot A, Dinov ID, Toga AW (2004) A myelo-architectonic method for the structural classification of cortical areas. NeuroImage 21:15–26.

Barth E, Zetzsche C, Ferraro M, Rentschler I (1993) Fractal properties from 2D-curvature on multiple scales. In: Geometric methods in computer vision (Vemuri B, ed), pp 87–99. Bellingham, WA: The International Society for Optical Engineering.

Bartley AJ, Jones DW, Weinberger DR (1997) Genetic variability of human brain size and cortical gyral patterns. Brain 120:257–269.

Bartzokis G, Sultzer D, Lu PH, Nuechterlein KH, Mintz J, Cummings JL (2004) Heterogeneous age-related breakdown of white matter structural integrity: implications for cortical "disconnection" in aging and Alzheimer's disease. Neurobiol Aging 25:843–851.

Bellugi U, Lichtenberger L, Jones W, Lai Z, St George M (2000) I. The neurocognitive profile of Williams syndrome: a complex pattern of strengths and weaknesses. J Cogn Neurosci 12[Suppl 1]:7–29.

Bullmore ET, Suckling J, Overmeyer S, Rabe-Hesketh S, Taylor E, Brammer MJ (1999) Global, voxel, and cluster tests, by theory and permutation, for a difference between two groups of structural MR images of the brain. IEEE Trans Med Imag 18:32–42.

Cabeza R, Nyberg L (2000) Imaging cognition II: an empirical review of 275 PET and fMRI studies. J Cogn Neurosci 12:1–47.

Cadigan KM, Nusse R (1997) Wnt signaling: a common theme in animal development. Genes Dev 11:3286–3305.

Duba HC, Doll A, Neyer M, Erdel M, Mann C, Hammerer I, Utermann G, Grzeschik KH (2002) The elastin gene is disrupted in a family with a balanced translocation t(7;16)(q11.23;q13) associated with a variable expression of the Williams-Beuren syndrome. Eur J Hum Genet 10:351–361.

Eckert MA, Hu D, Eliez S, Bellugi U, Galaburda AM, Korenberg JR, Mills D, Reiss AL (2005) Evidence for superior parietal impairment in Williams syndrome. Neurology 64:152–153.

Fischl B, Dale AM (2000) Measuring the thickness of the human cerebral cortex from magnetic resonance images. Proc Natl Acad Sci USA 97:11050–11055.

Galaburda AM, Bellugi U (2000) V. Multi-level analysis of cortical neuroanatomy in Williams syndrome. J Cogn Neurosci 12[Suppl 1]:74–88.

Galaburda AM, Schmitt JE, Atlas SW, Eliez S, Bellugi U, Reiss AL (2001) Dorsal forebrain anomaly in Williams syndrome. Arch Neurol 11:1865–1869.

Gogtay N, Giedd JN, Lusk L, Hayashi KM, Greenstein D, Vaitiuzis C, Nugent TF, Herman DH, Classen L, Toga AW, Rapoport JL, Thompson PM (2004) Dynamic mapping of human cortical development during childhood and adolescence. Proc Natl Acad Sci USA 101:8174–8179.

Grice SJ, de Haan M, Halit H, Johnson MH, Csibra G, Grant J, Karmiloff-Smith A (2003) ERP abnormalities of visual perception in Williams syndrome. NeuroReport 14:1773–1777.

Gu X, Wang YL, Chan T, Thompson PM, Yau ST (2003) Genus zero con-

formal mapping and its application to brain surface mapping. In: 18th international conference on information processing in medical imaging (IPMI2003): lecture notes in computer science, Vol 2732 (Taylor CJ, Noble JA, eds), pp 172–184. New York: Springer.

Haier RJ, Jung RE, Yeo RA, Head K, Alkire MT (2004) Structural brain variation and general intelligence. NeuroImage 23:425–433.

Hayashi KM, Thompson PM, Mega MS, Zoumalan CI, Dittmer SS (2002) Medial hemispheric surface gyral pattern delineation in 3D: surface curve protocol, http://www.loni.ucla.edu/~khayashi/Public/medial_surface/.

Holinger DP, Bellugi U, Mills DL, Bellugi U, Korenberg JR, Reiss AL, Sherman GF, Galaburda AM (2005) Relative sparing of primary auditory cortex in Williams syndrome. Brain Res 1037:35–42.

Jernigan TL, Bellugi U, Sowell E, Doherty S, Hesselink JR (1993) Cerebral morphologic distinctions between Williams and Down syndromes. Arch Neurol 50:186–191.

Jernigan TL, Archibald SL, Fennema-Notestine C, Gamst AC, Stout JC, Bonner J, Hesselink JR (2001) Effects of age on tissues and regions of the cerebrum and cerebellum. Neurobiol Aging 22:581–594.

Jones SE, Buchbinder BR, Aharon I (2001) Three-dimensional mapping of cortical thickness using Laplace's equation. Hum Brain Mapp 11:12–32.

Kanwisher N, McDermott J, Chun MM (1997) The fusiform face area: a module in human extrastriate cortex specialized for face perception. J Neurosci 17:4302–4311.

Karmiloff-Smith A, Grant J, Berthoud I, Davies M, Howlin P, Udwin O (1997) Language and Williams syndrome: how intact is "intact?" Child Development 68:246–262.

Karmiloff-Smith A, Tyler LK, Voice K, Sims K, Udwin O, Howlin P, Davies M (1998) Linguistic dissociations in Williams syndrome: evaluating receptive syntax in on-line and off-line tasks. Neuropsychologia 36:343–351.

Karmiloff-Smith A, Thomas M, Annaz D, Humphreys K, Ewing S, Brace N, Duuren M, Pike G, Grice S, Campbell R (2004) Exploring the Williams syndrome face-processing debate: the importance of building developmental trajectories. J Child Psychol Psychiatry 45:1258–1274.

Kiselev VG, Hahn KR, Auer DP (2003) Is the brain cortex a fractal? NeuroImage 20:1765–1774.

Korenberg JR, Chen XN, Hirota H, Lai Z, Bellugi U, Burian D, Roe B, Matsuoka R (2000) VI. Genome structure and cognitive map of Williams syndrome. J Cogn Neurosci 12[Suppl 1]:89–107.

Kosslyn SM (1994) Image and brain. Cambridge, MA: MIT.

Kruggel F, Bruckner MK, Arendt T, Wiggins CJ, von Cramon DY (2001) Analyzing the neocortical fine structure. In: Information processing in medical imaging (Insana MF, Leahy RM, eds), pp 239–245. New York: Springer.

Kulynych JJ, Luevano LF, Jones DW, Weinberger DR (1997) Cortical abnormality in schizophrenia: an *in vivo* application of the gyrification index. Biol Psychiatry 41:995–999.

Lerch JP, Evans AC (2005) Cortical thickness analysis examined through power analysis and a population simulation. NeuroImage 24:163–173.

Lerch JP, Pruessner JC, Zijdenbos A, Hampel H, Teipel SJ, Evans AC (2005) Focal decline of cortical thickness in Alzheimer's disease identified by computational neuroanatomy. Cereb Cortex, in press.

Lohmann G, Preul C, Hund-Georgiadis M (2003) Morphology-based cortical thickness estimation. Inf Process Med Imaging 18:89–100.

Luders E, Narr KL, Thompson PM, Rex DE, Jancke L, Toga AW (2004) Gender differences in cortical complexity. Nat Neurosci 7:799–800.

MacDonald D (1998) A method for identifying geometrically simple surfaces from three dimensional images. PhD thesis, McGill University.

Mazziotta JC, Toga AW, Evans AC, Fox PT, Lancaster J, Zilles K, Woods RP, Paus T, Simpson G, Pike B, Holmes CJ, Collins DL, Thompson PM, MacDonald D, Schormann T, Amunts K, Palomero-Gallagher N, Parsons L, Narr KL, Kabani N (2001) A probabilistic atlas and reference system for the human brain: International Consortium for Brain Mapping. Philos Trans R Soc Lond B Biol Sci 356:1293–1322.

Memoli F, Sapiro G, Thompson P (2004) Implicit brain imaging. NeuroImage 23 [Suppl 1]:S179–S188.

Mervis CB, Morris CA, Klein-Tasman BP, Bertrand J, Kwitny S, Appelbaum LG, Rice CE (2003) Attentional characteristics of infants and toddlers with Williams syndrome during triadic interactions. Dev Neuropsychol 23:243–268.

Meyer-Lindenberg A, Kohn P, Mervis CB, Kippenhan JS, Olsen RK, Morris CA, Berman KF (2004) Neural basis of genetically determined visuospatial construction deficit in Williams syndrome. Neuron 43:623–631.

Miller MI, Massie AB, Ratnanather JT, Botteron KN, Csernansky JG (2000) Bayesian construction of geometrically based cortical thickness metrics. NeuroImage 12:676–687.

Mills DL, Alvarez TD, St George M, Appelbaum LG, Neville H, Bellugi U (2000) Electrophysiological studies of face recognition in Williams syndrome. J Cogn Neurosci 12:S47–S64.

Narr KL, Bilder RM, Toga AW, Woods RP, Rex DE, Szeszko PR, Robinson D, Sevy S, Gunduz-Bruce H, Wang YP, DeLuca H, Thompson PM (2005) Mapping cortical thickness and gray matter concentration in first episode schizophrenia. Cereb Cortex, in press.

Ono M, Kubik S, Abernathey CD (1990) Atlas of the cerebral sulci. Stuttgart, Germany: Thieme.

Ratnanather JT, Botteron KN, Nishino T, Massie AB, Lal RM, Patel SG, Peddi S, Todd RD, Miller MI (2001) Validating cortical surface analysis of medial prefrontal cortex. NeuroImage 14:1058–1069.

Reiss AL, Eckert MA, Rose FE, Karchemskiy A, Kesler S, Chang M, Reynolds MF, Kwon H, Galaburda A (2004) An experiment of nature: brain anatomy parallels cognition and behavior in Williams syndrome. J Neurosci 24:5009–5015.

Reiss AL, Eliez S, Schmitt JE, Straus E, Lai Z, Jones W, Bellugi U (2000) IV. Neuroanatomy of Williams syndrome: a high-resolution MRI study. J Cogn Neurosci. 12[Suppl 1]:65–73.

Richman DP, Stewart RM, Hutchinson JW, Caviness VS (1975) Mechanical model of brain convolutional development. Science 189:18–21.

Rockel AJ, Hiorns RW, Powell TPS (1974) Numbers of neurons through full depth of neocortex. J Anat 118:371.

Ross ED, Mesulam MM (1979) Dominant language functions of the right hemisphere? Prosody and emotional gesturing. Arch Neurol 36:144–148.

Salmond CH, Ashburner J, Vargha-Khadem F, Connelly A, Gadian DG, Friston KJ (2002) Distributional assumptions in voxel-based morphometry. NeuroImage 17:1027–1030.

Schmitt JE, Eliez S, Bellugi U, Reiss AL (2001) Analysis of cerebral shape in Williams syndrome. Arch Neurol 58:283–287.

Schmitt JE, Watts K, Eliez S, Bellugi U, Galaburda AM, Reiss AL (2002) Increased gyrification in Williams syndrome: evidence using 3D MRI methods. Dev Med Child Neurol 44:292–295.

Shattuck DW, Sandor-Leahy SR, Schaper KA, Rottenberg DA, Leahy RM (2001) Magnetic resonance image tissue classification using a partial volume model. NeuroImage 13:856–876.

Sowell ER, Thompson PM, Rex D, Kornsand D, Tessner KD, Jernigan TL, Toga AW (2002a) Mapping sulcal pattern asymmetry and local cortical surface gray matter distribution *in vivo*: maturation in perisylvian cortices. Cereb Cortex 12:17–26.

Sowell ER, Thompson PM, Peterson BS, Mattson SN, Welcome SE, Henkenius AL, Riley EP, Jernigan TL, Toga AW (2002b) Mapping cortical gray matter asymmetry patterns in adolescents with heavy prenatal alcohol exposure. NeuroImage 17:1807–1819.

Sowell ER, Peterson BS, Thompson PM, Welcome SE, Henkenius AL, Toga AW (2003a) Mapping cortical change across the human life span. Nat Neurosci 6:309–315.

Sowell ER, Thompson PM, Welcome SE, Henkenius AL, Toga AW, Peterson BS (2003b) Cortical abnormalities in children and adolescents with attention-deficit hyperactivity disorder. Lancet 362:1699–1707.

Sowell ER, Thompson PM, Leonard CM, Welcome SE, Kan E, Toga AW (2004) Longitudinal mapping of cortical thickness and brain growth in normal children. J Neurosci 24:8223–8231.

Steinmetz H (1996) Structure, functional and cerebral asymmetry: *in vivo* morphometry of the planum temporale. Neurosci Biobehav Rev 20:587–591.

Thomas M, Karmiloff-Smith A (2000) Are developmental disorders like cases of adult brain damage? Implications from connectionist modelling. Behav Brain Sci 25:727–750.

Thompson PM, Schwartz C, Lin RT, Khan AA, Toga AW (1996) 3D statistical analysis of sulcal variability in the human brain. J Neurosci 16:4261–4274.

Thompson PM, Woods RP, Mega MS, Toga AW (2000) Mathematical/computational challenges in creating population-based brain atlases. Hum Brain Mapp 9:81–92.

Thompson PM, Mega MS, Woods RP, Blanton RE, Moussai J, Zoumalan CI, Aron J, Cummings JL, Toga AW (2001a) Early cortical change in Alzheimer's disease detected with a disease-specific population-based brain atlas. Cereb Cortex 11:1–16.

Thompson PM, Cannon TD, Narr KL, van Erp T, Khaledy M, Poutanen V-P, Huttunen M, Lönnqvist J, Standertskjöld-Nordenstam C-G, Kaprio J, Dail R, Zoumalan CI, Toga AW (2001b) Genetic influences on brain structure. Nat Neurosci 4:1253–1258.

Thompson PM, Hayashi KM, de Zubicaray G, Janke AL, Rose SE, Semple J, Herman D, Hong MS, Dittmer S, Doddrell DM, Toga AW (2003) Dynamics of gray matter loss in Alzheimer's disease. J Neurosci 23:994–1005.

Thompson PM, Hayashi KM, Sowell ER, Gogtay N, Giedd JN, Rapoport JL, de Zubicaray GI, Janke AL, Rose SE, Semple J, Doddrell DM, Wang YL, van Erp TGM, Cannon TD, Toga AW (2004) Mapping cortical change in Alzheimer's disease, brain development, and schizophrenia. NeuroImage 23[Suppl 1]:S2–S18.

Trauner DA, Bellugi U, Chase C (1989) Neurologic features of Williams and Down syndromes. Pediatr Neurol 5:166–168.

van Essen DC (1997) A tension-based theory of morphogenesis and compact wiring in the central nervous system. Nature 385:313–318.

Vogeley K, Schneider-Axmann T, Pfeiffer U, Tepest R, Bayer TA, Bogerts B, Honer WG, Falkai P (2000) Disturbed gyrification of the prefrontal region in male schizophrenic patients: a morphometric postmortem study. Am J Psychiatry 157:34–39.

Witelson SF, Kigar DL (1992) Sylvian fissure morphology and asymmetry in men and women: bilateral differences in relation to handedness in men. J Comp Neurol 323:326–340.

Yezzi A, Prince J (2001) A PDE approach for measuring tissue thickness. In: Computer vision and pattern recognition, pp 213–220. Berlin: Springer.

Zeineh MM, Engel SA, Thompson PM, Bookheimer S (2003) Dynamics of the hippocampus during encoding and retrieval of face–name pairs. Science 299:577–580.

Zhang K, Sejnowski TJ (2000) A universal scaling law between gray matter and white matter of cerebral cortex. Proc Natl Acad Sci USA 97:5621–5626.

Zhou Y, Thompson PM, Toga AW (1999) Automatic extraction and parametric representations of cortical sulci. Comput Graph Appl 19:49–55.

Zilles K, Armstrong E, Schleicher A, Kretschmann HJ (1988) The human pattern of gyrification in the cerebral cortex. Anat Embryol (Berl) 179:173–179.